
RETRIEVAL-BASED RECONSTRUCTION FOR TIME-SERIES CONTRASTIVE LEARNING

Maxwell A. Xu¹, Alexander Moreno², Hui Wei³, Benjamin M. Marlin³, James M. Rehg²

¹ Georgia Tech, ² UIUC, ³ UMass Amherst
maxxu@gatech.edu

ABSTRACT

The success of self-supervised contrastive learning hinges on identifying positive data pairs that, when pushed together in embedding space, encode useful information for subsequent downstream tasks. However, in time-series, this is challenging because creating positive pairs via augmentations may break the original semantic meaning. We hypothesize that if we can retrieve information from one subsequence to successfully reconstruct another subsequence, then they should form a positive pair. Harnessing this intuition, we introduce our novel approach: REtrieval-BAsed Reconstruction (REBAR) contrastive learning. First, we utilize a convolutional cross-attention architecture to calculate the REBAR error between two different time-series. Then, through validation experiments, we show that the REBAR error is a predictor of mutual class membership, justifying its usage as a positive/negative labeler. Finally, once integrated into a contrastive learning framework, our REBAR method can learn an embedding that achieves state-of-the-art performance on downstream tasks across various modalities.

1 INTRODUCTION

Self-supervised learning uses the underlying structure within a dataset to learn rich and generalizable representations without labels, enabling fine-tuning on various downstream tasks. This reduces the need for large labeled datasets, which makes it an attractive approach for the time-series domain. With the advancement of sensor technologies, it is increasingly feasible to capture a large volume of data, but the cost of data labeling remains high. For example, in mobile health, acquiring labels requires burdensome real-time annotation (Rehg et al., 2017). Additionally, in medical applications such as ECG analysis, annotation is costly as it requires specialized medical expertise.

Contrastive learning is a powerful self-supervised learning technique, which involves constructing and contrasting positive and negative pairs to yield an embedding space that captures semantic relationships. To be successful, the process for generating such pairs should capture important structural properties of the data. In the vision applications that have driven this approach, augmentations are used to construct a positive pair by exploiting well-established invariances of the imaging process (e.g. flipping, rotating). Unfortunately, general time-series do not possess a large and rich set of such invariances. Shifting, which addresses translation invariance, is widely-used, but other common augmentations such as shuffling or scaling can destroy the signal semantics. For example, shuffling an ECG waveform destroys the temporal structure of the QRS complex, and scaling it can change the clinical diagnosis (Nault et al., 2009). Moreover, there is no consistent consensus of augmentations in the literature; methods such as TF-C (Zhang et al., 2022) incorporate jittering and scaling, while TS2Vec (Yue et al., 2022) finds that these augmentations impair downstream performance.

In this work, we introduce a novel approach for identifying positive and negative pairs for contrastive time-series learning through a "motif-based" retrieval and reconstruction method. In our framework, we define a time-series as being a composition of a series of subsequences, each of which has a class label. This conceptualization describes many real-world physiological signals. For example, a participant wearing an accelerometer sensor generates a time-series over the course of a day, which consists of a series of contiguous subsequences. Each subsequence has an individual activity label (e.g. sitting or walking) and contains brief temporal shapes or "motifs" that are generated from that specific activity class. This idea that the specific motifs within the subsequence are class-

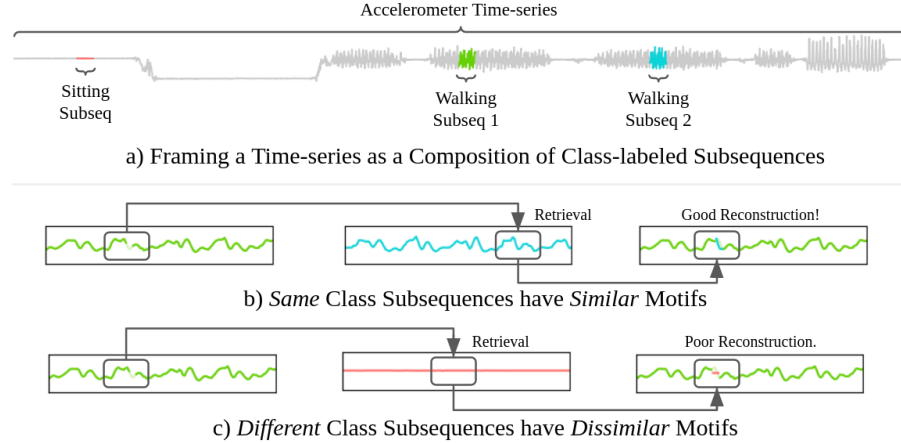


Figure 1: This figure demonstrates the intuition of our REtrieval-BAsed Reconstruction (REBAR) approach. If we can successfully retrieve motifs from another subsequence to aid in reconstruction, then the two subsequences should form a positive pair in a contrastive learning framework. This is because subsequences of the same class are likely to share similar motifs for retrieval. b) shows that when Walking Subseq 1 is missing a point, we can identify a similar double peak motif from Walking Subseq 2 to achieve a good retrieval-based reconstruction. In c), the Sitting Subseq has no matching motif, leading to a poor reconstruction.

discriminative is widely-studied and validated throughout the time-series data-mining literature (Yeh et al., 2018; 2016; Alaee et al., 2021; Li, 2021), and so, two subsequences with similar motifs should be a good candidate to form a positive pair. Additionally, framing our work in the context of time-series signals that model an changing state over time, allow us to leverage and benchmark sampling-based contrastive learning approaches, such as TNC (Tonekaboni et al., 2021), in which a positive pairs are sampled directly from the original long time-series.

In our REtrieval-BAsed Reconstruction (REBAR)¹ approach, we propose to measure the similarity between two subsequences by retrieving motifs in one subsequence conditioned on the unmasked motifs in the other, to reconstruct the other subsequence’s masked-out points. The ensuing reconstruction error is a quasi-distance measure that captures motif similarity. Pairs with a closer distance can then form positive examples in contrastive learning. We illustrate this idea in Fig. 1. Because the pair is likely to share the same class label (which we validate prior to contrastive learning), then the resulting learned embedding space is likely to be class-discriminative. We are able to demonstrate this by showing that the embedding space achieves SOTA classification results with both a linear probe and in clusterability evaluations. Our main contributions in this work are:

1. We introduce a novel method of identifying positives and negative pairs for time-series contrastive learning with our REBAR metric, calculated from a convolutional cross-attention architecture that does between-sequence retrieval and comparison of potential class-specific motifs.
2. To justify this approach and as a prerequisite to contrastive learning, we demonstrate that the REBAR metric predicts mutual class membership of two subsequences.
3. Our REBAR contrastive learning approach achieves state-of-the-art performance against a representative suite of contrastive learning methods on a diverse set of time-series sensor data that are composed of a series of class-labeled subsequences

2 RELATED WORKS

Augmentation-based Contrastive Learning: Augmentation-based methods are the most studied type of contrastive learning method in time-series research, due to the success of augmentation-based strategies in computer vision (He et al., 2020; Chen et al., 2020; Chen & He, 2021; Caron et al., 2021). However, it is unclear which augmentation strategies are most effective for time-series, and the findings across different works are inconsistent. TS2Vec (Yue et al., 2022) uses cropping and masking to create positive examples, and their ablation study found that jittering, scaling, and

¹Note that we will interchangeably use "REBAR" to refer to the REBAR contrastive learning approach, the REBAR cross-attention, and the REBAR metric. The specific meaning will be evident from the context.

shuffling augmentations led to performance drops. Conversely, TF-C (Zhang et al., 2022) included jittering and scaling, along with cropping, time-shifting, and frequency augmentations. TS-TCC (Eldele et al., 2023) augments the time-series with either jittering+scaling or jittering+shuffling. This is in spite of how shuffling breaks temporal dependencies, and scaling changes the semantic meaning of a bounded signal. Other augmentation works (Woo et al., 2022; Yang & Hong, 2022; Yang et al., 2022b; Ozyurt et al., 2022; Lee et al., 2022) also use some combination of scaling, shifting, jittering, or masking. Empirical performance was used to justify the augmentation choice, but differences in datasets, architectures, and training regimes make it difficult to draw a clear conclusion. Our REBAR method uses an alternative approach to generate positive/negative pairs not based on augmentation.

Sampling-based Contrastive Learning: After sampling an anchor subsequence, TLoss (Franceschi et al., 2019) creates the positive subsequence as a crop of the anchor and the negative as a crop from a different time-series. CLOCS (Kiyasseh et al., 2021) samples pairs of temporally-adjacent subsequences and pairs of subsequences across channels from the same time-series as positives. TNC (Tonekaboni et al., 2021) randomly samples a positive example from the anchor subsequence’s neighborhood region and an unlabeled example from outside. The neighborhood is found via a stationarity test, resulting in TNC’s run-time being 250x slower than TS2Vec (Yue et al., 2022), and it utilizes a hyperparameter to estimate the probability that the unlabeled example is a true negative. Our REBAR approach is sampling-based, but unlike previous work, our positive examples are not selected based on temporal proximity to the anchor. Instead, positive examples are selected on the basis of their similarity to the anchor, measured by retrieval-based reconstruction.

Other Self-supervised Learning Methods: CPC is a contrastive learning method that trains an autoregressive model and learns to contrast future points against incorrect ones (Oord et al., 2018). There have also been contrastive learning methods designed for specific time-series modalities that use expert knowledge, such as for EEG (Zhang et al., 2021). Another method is the Masked Autoencoder (MAE), which is used in both NLP (Devlin et al., 2018) and Vision (He et al., 2022), and a few works have adapted it to time-series (Cheng et al., 2023; Li et al., 2023). These models typically utilize transformers to encode the masked input before using a lightweight decoder for reconstruction. While both REBAR and MAEs involve masked reconstruction, the fundamental approaches differ substantially. REBAR estimates if a pair of subsequences are of the same class through a paired reconstruction error, and then uses this to contrast subsequences. In comparison, MAEs learn between-time-point interactions within a subsequence by learning a reconstruction as a composition of the unmasked data, and are not designed to explicitly compare subsequences.

Retrieval-based Cross-Attention: Our retrieval-based reconstruction model utilizes a cross-attention mechanism to retrieve information across different subsequences for comparison, and there are other related works that utilize cross-attention retrieval. The most common usage is for cross-modality, in which text is the query to retrieve relevant regions in an image (Lee et al., 2018; Miech et al., 2021; Zheng et al., 2022). Cross-attention in NLP has been used to assess semantic similarity (Li et al., 2020; Hao et al., 2017) and to provide augmentations while training another model in a Q&A task (Yang et al., 2020). In time-series, cross-attention has been used to retrieve the most salient information from a signal (Garg & Candan, 2021) and to retrieve time-series to aid forecasting (Yang et al., 2022a). Although there are self-supervised works that use retrieval for evaluation (Chen et al., 2021; Ma et al., 2022; Wang et al., 2022), these are very different from REBAR, in which a retrieval-based method is used to directly train the self-supervised learning approach.

Time-series Motifs: In our framing of class-labeled subsequences that make up the longer time-series, we define a motif as a shorter series within a subsequence that repeats itself approximately across the time-series. Much work has been done in identifying class-discriminative motifs via works such as matrix profile (Yeh et al., 2016; 2018; Gharghabi et al., 2018), and there are many classical time-series approaches that use template-matching methods to classify (Frank et al., 2012; Okawa, 2019; Niennattrakul et al., 2012). Our REBAR method uses our cross-attention model to retrieve motifs that are useful in the context of reconstruction. Then, we can utilize the reconstruction error to capture motif-similarity in novel contrastive learning context for identifying positive pairs.

3 METHOD

We frame our paper around time-series, $\mathbf{A} \in \mathbb{R}^{U \times D}$ where U is length and D is channel, which are composed of class-labeled subsequences. A subsequence is $\mathbf{X} \in \mathbb{R}^{T \times D}$ with $T \ll U$, such that

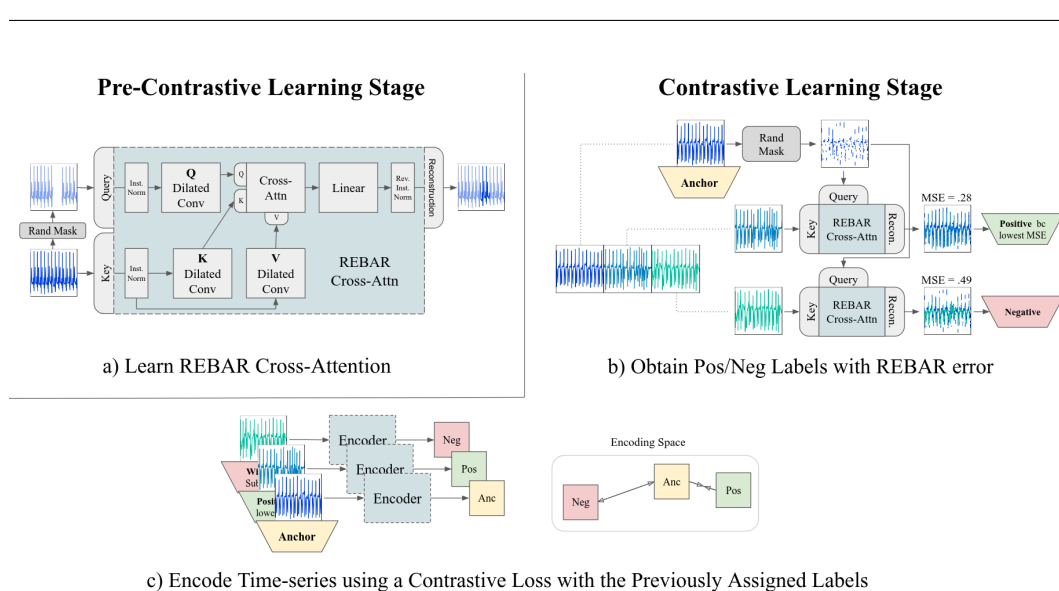


Figure 2: a) First, our REBAR cross-attention is trained to retrieve information from the key to reconstruct a masked-out query. b) Next, it is frozen and utilized to identify positive/negative labels. After sampling subsequences from the time-series, the subsequence that reconstructed the anchor with the lowest REBAR error is labeled as positive, and the others are labeled as negative. c) After encoding each of these subsequences, we use the assigned labels within a contrastive loss function.

$\mathbf{A}[i : i + T] = \mathbf{X}$ for some i . Then, $y(\mathbf{X})$ is the true class label of \mathbf{X} . For example, walking subsequence labels within a HAR time-series. This notation will be used throughout the paper.

Our approach utilizes retrieval-based reconstruction, REBAR, as a metric for contrastive learning, as it is a strong predictor for mutual class membership between subsequences. Our key idea is that if two subsequences (e.g. \mathbf{X}_q and \mathbf{X}_k) are instantiations of the same class label, then they are likely to share similar temporal shapes and patterns. This is corroborated by the extensive time-series motif literature, which seeks to classify time-series by identifying class-discriminative motifs (Yeh et al., 2018; 2016; Alaee et al., 2021; Li, 2021), as well as our validation experiments found later in Sec.3.4. We design our REBAR model to reconstruct $\bar{\mathbf{X}}_q$ (where bar designates masked) by retrieving motifs in \mathbf{X}_k that match the unablated context in $\bar{\mathbf{X}}_q$. Then, the ensuing reconstruction error serves as a quasi-distance metric between two subsequences to guide positive/negative pair construction, shown below in Eq 1.

$$d(\mathbf{X}_q, \mathbf{X}_k) = \|\text{REBAR}(\bar{\mathbf{X}}_q, \mathbf{X}_k) - \mathbf{X}_q\|_2^2 \quad (1)$$

Thus, we hypothesize that if $d(\mathbf{X}_q, \mathbf{X}_k)$ is small, then it predicts if $y(\mathbf{X}_q) = y(\mathbf{X}_k)$. While not a valid distance metric (violating symmetry and the triangle inequality), positivity is likely to hold, as we would need perfect reconstruction for it not to, and we can train REBAR to approximate the distance from a sequence to itself is (approximately) zero.

The full REBAR contrastive learning approach is shown in Fig. 2. Sec. 3.1 describes our cross-attention module for learning the REBAR metric, Sec. 3.2 and Sec. 3.3 explains how to train and apply the model for subsequence comparison in a contrastive learning framework. Sec. 3.4 investigates the assumption that REBAR error predicts mutual class membership.

3.1 DESIGN OF THE REBAR CROSS-ATTENTION

Retrieval-based reconstruction retrieves the most useful information in one subsequence to reconstruct another. Cross-attention learns to produce weighted averages of a transformation of the key time-series, and is an attractive method for modeling this paradigm. This is because the weights are a learned similarity between the query and keys and can be interpreted as a retrieval function. We describe our REBAR cross-attention model with a retrieval formulation below:

$$\text{REBAR}(\bar{\mathbf{X}}_q; \mathbf{X}_k) = \sum_{\mathbf{x}_k \in \mathbf{X}_k} \frac{\exp(\langle f_q(\bar{\mathbf{X}}_q), f_k(\mathbf{x}_k) \rangle)}{\sum_{\mathbf{x}'_k \in \mathbf{X}'_k} \exp(\langle f_q(\bar{\mathbf{X}}_q), f_k(\mathbf{x}'_k) \rangle)} f_v(\mathbf{x}_k) \quad (2)$$

$$= \sum_{\mathbf{x}_k \in \mathbf{X}_k} p(\mathbf{x}_k | \bar{\mathbf{X}}_q) f_v(\mathbf{x}_k) \quad (3)$$

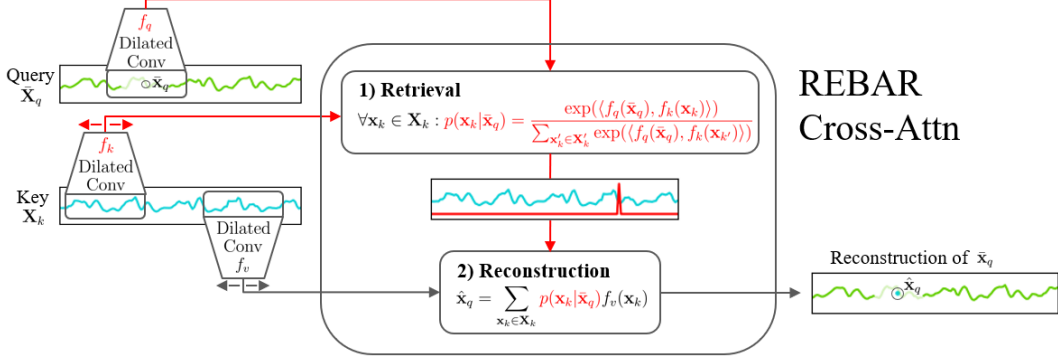


Figure 3: Visualization of REBAR Cross-attention’s reconstruction of a single masked-out point \bar{x}_q , $\text{REBAR}(\bar{x}_q; \bar{X}_k)$. The red color designates the functions used for the attention weight calculation. In 1), the attention weights identify which region in \bar{X}_k should be retrieved for reconstruction by comparing the unmasked context around \bar{x}_q via the f_q dilated convolution, with the motifs in \bar{X}_k via the f_k dilated convolution. In 2), the attention weights are used to retrieve a f_v transformation of the key in a weighted average for reconstruction. Minor model details (e.g. norms) omitted for brevity.

where $f_q(\bar{x}_q) = \bar{x}_q \mathbf{W}_q$, $f_k(\mathbf{x}_k) = \mathbf{x}_k \mathbf{W}_k$, $f_v(\mathbf{x}_k) = \mathbf{x}_k \mathbf{W}_v$, and $\mathbf{W}_{\{q/k/v\}} \in \mathbb{R}^{D_x \times D}$ in vanilla cross-attention. \mathbf{W} is a learnable weight. $\bar{X}_k \in \mathbb{R}^{T \times D_x}$ is the key subsequence. $\bar{x}_q^\top \in \mathbb{R}^{D_x}$ is a row in $\bar{X}_q \in \mathbb{R}^{T \times D_x}$, the query subsequence, \bar{X}_q . Bar designates that the sequence is masked. The cross-attention’s scaling factor, biases, norms, and aggregation linear layer are omitted for brevity.

$p(\mathbf{x}_k|\bar{x}_q)$ in Eq. 3 is the retrieval function, which identifies regions in the key subsequence useful for the reconstruction downstream task based on the $\langle f_q(\bar{x}_q), f_k(\mathbf{x}_k) \rangle$ calculation found in Eq. 2. However, vanilla $f_{k/q}$ in the original transformer paper (Vaswani et al., 2017) is calculated with only a single time-point, which holds limited information about its semantic content. We would instead like our retrieval-function to retrieve motifs for reconstruction, so that reconstruction performance is directly dependent on motif-similarity. Therefore, we utilize a dilated convolution for $f_{k/q/v}$ to capture information from the wider surrounding temporal neighborhood (Xu et al., 2022). The $f_{k/q}$ dilated convs allow for motif-similarity comparison to identify regions in \bar{X}_k for retrieval, and then the f_v consolidates information from that region for reconstruction. The reversible instance norm (RevIN) (Kim et al., 2021) normalizes the data at input, before reversing it at the output for reconstruction. We opt to not use positional encoding so that the retrieval function focuses on learning a good motif comparison function, rather than considering specific positions of the motifs. The full block diagram is shown in 2a), and further model details can be found in Appendix A.1.1.

The retrieval and reconstruction steps of our $\text{REBAR}(\bar{X}_q, \bar{X}_k)$ cross-attention is visualized in Fig. 3. Our objective is to learn a good retrieval function, $p(\mathbf{x}_k|\bar{x}_q)$ that measures similarity of temporal structures between \bar{X}_q and \bar{X}_k . Therefore, we would like to avoid learning a complex model that may achieve an accurate reconstruction even when \bar{X}_q and \bar{X}_k are dissimilar. As such, we intentionally utilize a simple approach. *The query subsequence is not directly used for this reconstruction, it is only used to identify regions in the key subsequence to retrieve with $p(\mathbf{x}_k|\bar{x}_q)$.* The reconstruction information only flows from the retrieved regions of the key subsequence with $f_v(\mathbf{x}_k)$ forcing the model to learn how to effectively retrieve and compare motifs between subsequences rather than learning temporal dependencies within the query.

3.2 TRAINING REBAR CROSS-ATTENTION

In the pre-contrastive learning stage, we would like to train $\text{REBAR}(\bar{X}_q, \bar{X}_k)$ to learn how to effectively retrieve and reconstruct class-discriminative motifs across subsequences. However, we do not have $y(\cdot)$, so given a random \bar{X}_q, \bar{X}_k pair, it is unclear whether we want to minimize or maximize $d(\bar{X}_q, \bar{X}_k)$. Therefore, we train $\text{REBAR}(\bar{X}_q, \bar{X}_k)$ with $\bar{X}_q = \bar{X}_k$ because $y(\bar{X}_q) = y(\bar{X}_k)$ when $\bar{X}_q = \bar{X}_k$. The key has exactly the information that the query is missing, so we expect our model to learn how to retrieve the exact matching region in the key.

Next, we identify an effective masking strategy so that $\text{REBAR}(\bar{X}_q, \bar{X}_k)$ can learn to retrieve and reconstruct class-specific motifs (e.g. heartbeat in ECG (Schäfer & Leser, 2022)). We define a binary mask as $m \in \mathbb{R}^T$ with missing as 1 and not-missing as 0. We then investigate two types of

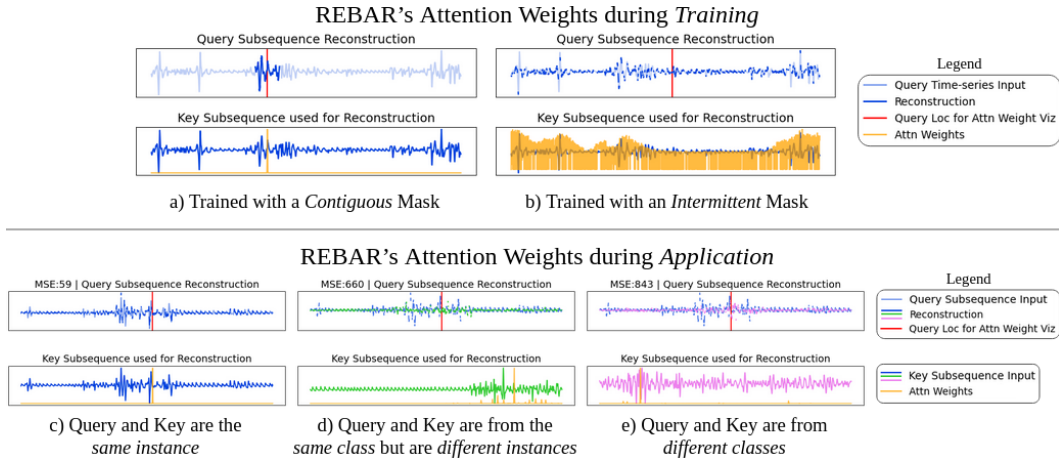


Figure 4: [top] a) A contiguous mask encourages REBAR to learn attention weights that are specific to the corresponding motif in the key. Conversely, with an intermittent mask, b), the attention is diffused and attends to transient motifs throughout the key. Specific attention weights allow for an effective comparison of class-discriminative motifs, so we utilize a contiguous mask for training. [bottom] We use an intermittent mask during application to evaluate motif similarity on a wider range of motifs present throughout the query, and the sparse attention in c) d) e) show that the model is still conducting specific motif comparison. c) and d) utilize keys that differ from the query, but our REBAR cross-attention still retrieves the most relevant information in the key for query reconstruction. The attention weights are conditioned on a masked-out downwards dip in the query, and each of the weights in c) d) e) are highest for a corresponding dip in the key. d)'s key is in the same class as the query, and the corresponding MSE is lower than e)'s.

masks: *contiguous* and *intermittent*. A contiguous mask is where a contiguous segment of length n is randomly masked out (i.e. $m[i : i + n] = 1$ with $i \in_R \{0, 1, \dots, T - n\}$ and \in_R is random sampling without replacement). An intermittent mask is where n time stamps are randomly masked out (i.e. $m[i_1] = 1, \dots, m[i_n] = 1$ for $i_1, \dots, i_{n-1} \in_R \{0, \dots, T\}$). Fig. 4b) shows that training with the intermittent mask results in a dispersed attention distribution, which means that the model is retrieving minor, non-unique motifs. Even if two signals originate from two different classes, we would be able to retrieve this non-unique motif from both signals, so the reconstruction performance would not be class-discriminative. Fig. 4a) shows that the attention weights learned with a contiguous mask fit exactly onto the region in the key corresponding to the masked region in the query, and thus the model has learned to retrieve specific motifs useful for reconstruction. Because the REBAR model has learned to compare specific motifs between the query and key, when comparing class-discriminative motifs, the ensuing reconstruction performance will be class-discriminative.

3.3 APPLYING OUR REBAR METRIC IN CONTRASTIVE LEARNING

Now, the trained REBAR cross-attention can be used to attempt to reconstruct $\bar{\mathbf{X}}_{\text{anchor}}$ from \mathbf{X}_{cand} in which $\mathbf{X}_{\text{anchor}} \neq \mathbf{X}_{\text{cand}}$. As previously discussed, the subsequent reconstruction error acts as a proxy for mutual class membership due to the motif retrieval and reconstruction properties, and it is validated empirically in Sec. 3.4. Thus, the REBAR metric can be used within a contrastive learning framework to identify if an anchor and a candidate should form a positive or negative pair. From the time-series \mathbf{A} , we uniformly random sample an anchor subsequence, $\mathbf{X}_{\text{anchor}}$, and n candidate subsequences, \mathbf{X}_{cand} , which make up the set $\mathcal{S}_{\text{cand}}$. Then, we can label the candidates as:

$$\mathbf{X}_{\text{pos}} = \underset{\mathbf{X}_{\text{cand}} \in \mathcal{S}_{\text{cand}}}{\operatorname{argmin}} d(\mathbf{X}_{\text{anchor}}, \mathbf{X}_{\text{cand}}) \quad (4)$$

$$\mathcal{S}_{\text{neg}} = \mathcal{S}_{\text{cand}} \setminus \{\mathbf{X}_{\text{pos}}\} \quad (5)$$

We can then use these labels with the NT-Xent loss (Chen et al., 2020), \mathcal{L} , shown below. τ is the temperature parameter and $\text{sim}(\cdot, \cdot)$ is the cosine similarity function.

$$\mathcal{L} = \frac{\exp(\text{sim}(\mathbf{X}_{\text{anchor}}, \mathbf{X}_{\text{pos}})/\tau)}{\exp(\text{sim}(\mathbf{X}_{\text{anchor}}, \mathbf{X}_{\text{pos}})/\tau) + \sum_{\mathbf{X}_{\text{neg}} \in \mathcal{S}_{\text{neg}}} \exp(\text{sim}(\mathbf{X}_{\text{anchor}}, \mathbf{X}_{\text{neg}})/\tau)} \quad (6)$$

This loss learns to pull the anchor and the subsequence that is most likely to be of the same class as the anchor, according to REBAR, together in the embedding space, while pushing the pairs that

are less likely apart. This allows us to capture the differences in class labels between different subsequences in our embedding space. During application, we use an intermittent mask. Fig. 4 shows that the model trained with a contiguous mask still maintains a sparse attention when applied with an intermittent mask, and so, the query is still reconstructed based on specific motifs from the key. Because the masked points are dispersed in an intermittent mask, we can evaluate motif-similarity via REBAR throughout the query for a better comparison with the key. This masking idea is further explained and empirically validated in Appendix A.1.2.

3.4 REBAR VALIDATION EXPERIMENTS

Before integrating the REBAR metric into a contrastive learning framework to identify positive/negative pairs, we assess whether the positive/negative pairs are meaningful by evaluating whether the metric effectively predicts mutual class membership. From the time-series, we randomly segment out one anchor subsequence, $\mathbf{X}_{\text{anchor}}$ and C candidate subsequences, $\mathbf{X}_{\text{cand}}^0, \dots, \mathbf{X}_{\text{cand}}^C$, from each of the C classes. Then, the anchor subsequence’s class is predicted to be the class of the candidate that provided the lowest REBAR error (i.e. $\text{pred}(\mathbf{X}_{\text{anchor}}) = \text{argmin}_i d(\mathbf{X}_{\text{anchor}}, \mathbf{X}_{\text{cand}}^i)$). The above procedure is then bootstrapped and repeated for each time-series to obtain an average of the class prediction accuracy. The results are shown in the confusion matrices in Fig. 5 below.

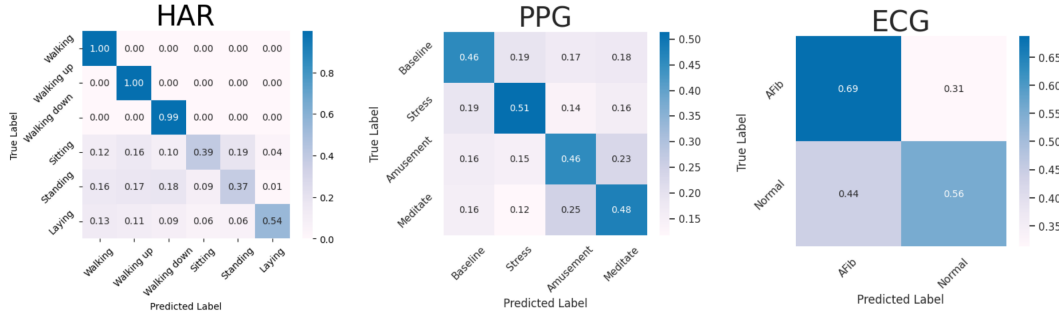


Figure 5: The high concentration on the diagonal observed across our datasets demonstrates that REBAR, although it is trained with a reconstruction task without class labels, is able to predict mutual class membership. This validates our approach for using REBAR to identify positive/negative pairs in contrastive learning. The different classes in HAR are arguably more distinctive than the classes for ECG and PPG, which can be seen in Appendix A.2, lending itself to the better performance.

Additionally, Fig. 4 visualizes the reconstruction of an anchor subsequence with different candidate subsequences along with its attention weights. Fig. 4b) and c) show that despite being trained with the key and the query being the same instance, REBAR model is still able to reconstruct the query when the key is different. The attention weights retrieve the most relevant information from the key, and the weights being sparse indicates that specific motifs are being retrieved and compared.

4 EXPERIMENTAL DESIGN

Benchmarks: Each benchmark is chosen to represent a specific time-series contrastive learning modeling paradigm with further details found in Appendix A.3. TS2Vec is one of the current SOTA methods that learns time-stamp level representations with augmentations; TNC samples a nearby subsequence as a positive and utilizes a hyperparameter to estimate whether a faraway sample is negative; CPC contrasts future predictions; SimCLR contrasts the most common augmentations (i.e. shifting, scaling, jittering); sliding-MSE is a simplified version of REBAR that uses a sliding MSE comparison as metric for evaluating pairwise similarity. We aim to assess how differing contrastive learning methods perform, so the encoder (Yue et al., 2022) is kept as a control across all baselines.

Data: We utilize 3 datasets from 3 different sensor domains with time-series that have their classification labels change over time: HAR to measure activity, PPG to measure stress, and ECG to measure heart condition. Each of these signals have drastically different structures, and the class-specific temporal patterns vary differently within a modality (e.g. in HAR, differences in labels manifest via amplitude differences; in ECG, differences in labels manifest via frequency differences). Please find further dataset descriptions and details in Appendix A.2

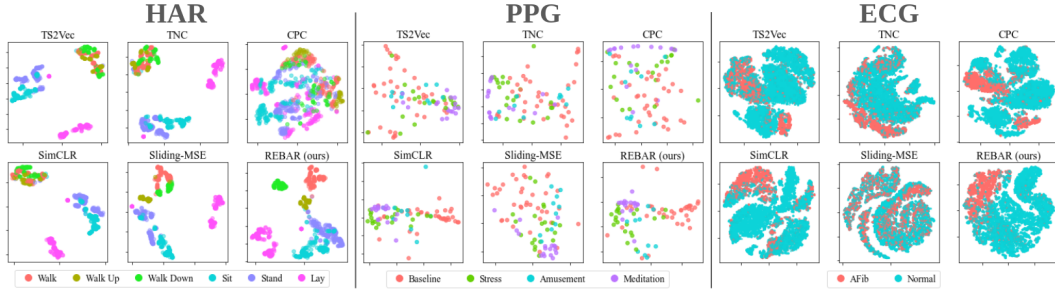


Figure 6: Qualitative Clusterability Results with t-SNE Visualizations

Downstream Evaluation: To evaluate their class-discriminative strengths, we learn a linear probe (i.e. logistic regression) on each model’s frozen encoding to perform downstream classification and use the Accuracy, AUROC, and AUPRC metrics to quantify the results. Additionally, a fully supervised model composed of an identical encoder as the baselines with a linear classification layer is benchmarked. This matches the linear probe evaluation for each of our baselines, only trained end-to-end. We then also assess cluster agreement for further corroboration. After a k -means clustering of the frozen encoding, with k as the number of classes, we assess the similarity of these clusters with the true labels with the Adjusted Rand Index and Normalized Mutual Information metrics.

5 RESULTS

Linear Probe Classification: Tbl. 1 shows that the linear probe trained on our REBAR representation consistently achieved the strongest results, even beating the fully supervised model in PPG and HAR, achieving the same accuracies, but higher AUROC and AUPRC. This demonstrates our REBAR’s methods strength in learning a representation that is better at handling class imbalance than the fully-supervised model. All of the contrastive learning methods struggle in the ECG domain because none of the models explicitly encode frequency information: the ECG class difference presents itself as abnormal vs. normal heartbeats frequency.

Our REBAR method demonstrates a much stronger performance than Sliding-MSE, showing the necessity of learning a retrieval-reconstruction distance rather than using a simple metric to identify positive pairs. Our improved performance compared to TNC highlights the value of identifying positives that are not necessarily near the anchor. The SimCLR’s poor results in PPG and ECG underscore the non-trivial nature of designing an augmentation-based method, even when such augmentations are common. Although TS2Vec is a SOTA method for contrastive learning, it is unable to consistently achieve strong performance. We suspect that this is because TS2Vec was evaluated on short class-labeled time-series rather than time-series with class-labeled subsequences. The other sampling-based methods (i.e. TNC, Sliding-MSE, REBAR) successfully exploit this structure to sample positive pairs from subsequences across the time to achieve stronger performance.

Model	PPG			HAR			ECG		
	Accuracy	AUROC	AUPRC	Accuracy	AUROC	AUPRC	Accuracy	AUROC	AUPRC
Fully Supervised	0.4138	0.6241	0.3689	0.9535	0.9835	0.9531	0.8480	0.8799	0.8350
TS2Vec	0.4023	0.6428	0.3959	0.9324	0.9931	0.9766	0.6889	0.7251	0.6617
TNC	0.2989	0.6253	0.3730	0.9437	0.9937	0.9788	0.7175	0.8429	0.7793
CPC	0.3448	0.5843	0.3642	0.8662	0.9867	0.9438	0.6856	0.6855	0.6369
SimCLR	0.3448	0.6119	0.3608	0.9465	0.9938	0.9763	0.6752	0.6618	0.5982
Sliding-MSE	0.3333	0.6456	0.3831	0.9352	0.9931	0.9767	0.6858	0.7292	0.6345
REBAR (ours)	0.4138	0.6977	0.4457	0.9535	0.9965	0.9891	0.7928	0.8462	0.8051

Table 1: Linear Probe Classification Results with Accuracy, AUROC, and AUPRC

Clusterability Evaluation: Tbl. 2 shows that when measuring the cluster agreement with the true class labels, REBAR continues to achieve the best ARI and NMI, corroborating the strong classification results. This is unlike other methods, such as TS2vec in PPG, that achieve strong linear probe results, but low cluster agreement. Fig. 6 above shows the t-SNE visualizations for all baselines across all three domains to help further illustrate the results of our clusterability experiment. In HAR, all methods except for REBAR group walk, walk up, and walk down together. In PPG, all of the methods have poor clustering, but REBAR seems to perform the best, with only the Meditation label being not clearly disjoint. In ECG, REBAR continues to have the best intra-class clustering.

Model	PPG		HAR		ECG	
	ARI	NMI	ARI	NMI	ARI	NMI
TS2Vec	-0.0353	0.1582	0.4654	0.6115	0.0251	0.0193
TNC	0.0958	0.1666	0.4517	0.5872	-0.0302	0.1009
CPC	0.1110	0.1867	0.1603	0.2217	0.0239	0.0169
SimCLR	0.1535	0.3081	0.5805	0.6801	-0.0372	0.1157
Sliding-MSE	0.1083	0.2141	0.5985	0.7019	-0.0081	0.0005
REBAR (ours)	0.1830	0.3422	0.6258	0.7721	0.4194	0.2696

Table 2: Clusterability Results with Adjusted Rand Index and Normalized Mutual Information

REBAR approach analysis: Fig. 7 visualizes the positive pairing from the list of candidates for a given anchor that was identified by our REBAR method with Eq. 4. We see that even when there is no exact match of the anchor within the candidates, REBAR’s motif-comparison retrieval and reconstruction is able to identify a positive example from the candidates that shares the same class as the anchor. Then, as according to Eq. 5, our negative examples are the remaining candidates. Our method is effective in identifying positive examples that will learn a class-discriminative space. We include a much larger gallery of such positive pairing visualizations in Appendix A.5

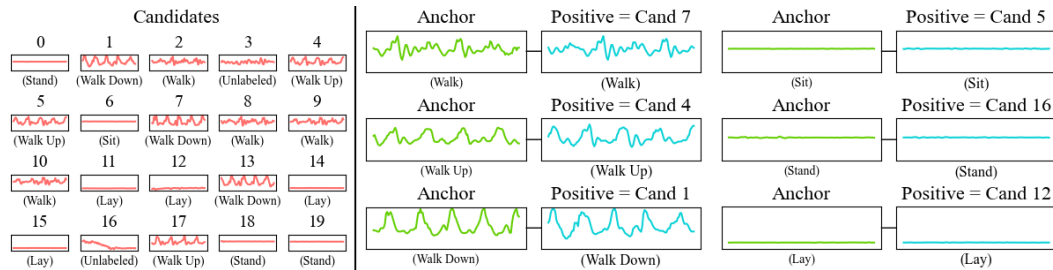


Figure 7: Positive pairings identified by REBAR from the candidates, for an anchor of each class.

Tbl. 3 demonstrates that each of the model design contributes to REBAR’s strong contrastive learning performance, especially the dilated convolutions. This makes sense because the dilated convolutions are what enable the motif comparison and retrieval. Additionally, REBAR is fairly robust against hyperparameter tuning. When we modify the size of the dilated conv’s receptive field or the size of contiguous masks, the downstream linear probe and clusterability performance remains consistent. We also see that our model is also robust to REBAR cross-attention reconstruction training epochs. See Appendix A.1 for further analysis and model details.

	Acc	AUROC	AUPRC	ARI	NMI
Baseline at Epoch 300, Mask=15, RF=43					
REBAR	0.9535	0.9965	0.9891	0.6258	0.7721
Ablation (Lower is better)					
w/o DilatedConv	0.8930 (-0.061)	0.9839 (-0.130)	0.9302 (-0.059)	0.2845 (-0.341)	0.5094 (-0.263)
w/o RevIN	0.9451 (-0.008)	0.9958 (-0.001)	0.9861 (-0.003)	0.5613 (-0.065)	0.6450 (-0.127)
w/ PosEmbed	0.9479 (-0.006)	0.9957 (-0.001)	0.9863 (-0.003)	0.5550 (-0.071)	0.6522 (-0.120)
Robustness (Equal or Higher is better)					
REBAR at Epoch 100	0.9592 (+0.006)	0.9970 (+0.000)	0.9900 (+0.001)	0.6169 (-0.009)	0.7589 (-0.013)
REBAR at Epoch 200	0.9592 (+0.006)	0.9967 (+0.000)	0.9896 (+0.001)	0.6830 (+0.057)	0.8425 (+0.070)
REBAR w/ Mask=5	0.9493 (-0.004)	0.9963 (+0.000)	0.9881 (-0.001)	0.6120 (-0.014)	0.7550 (-0.017)
REBAR w/ Mask=25	0.9592 (+0.006)	0.9962 (+0.000)	0.9873 (-0.002)	0.6484 (+0.023)	0.7891 (+0.017)
REBAR w/ RF=31	0.9507 (-0.003)	0.9962 (+0.000)	0.9881 (-0.001)	0.6390 (+0.013)	0.7787 (+0.007)
REBAR w/ RF=55	0.9380 (-0.016)	0.9943 (-0.002)	0.9794 (-0.010)	0.6570 (+0.031)	0.8090 (+0.037)

Table 3: REBAR model Ablation Study and Hyperparameter Analysis on HAR data

6 CONCLUSION

Our Retrieval-Based Reconstruction is a novel approach to time-series contrastive learning. By using cross-attention to retrieve motifs in one subsequence to reconstruct class-specific shapes in another, we can predict mutual class membership. Then, if we use this REBAR metric to identify positive and negative pairs, we are able to achieve state-of-the-art results in learning a class discriminative embedding space. Our REBAR method offers a new approach on how to identify positive pairings in time-series that are composed of a series of class-labeled subsequences, and we hope that this work will drive future research into understanding how to best learn representations in time-series and the greater contrastive learning space.

7 ETHICS STATEMENT

Our paper works on creating models for health-related signals, and it has the potential to improve health outcomes, but at the same time could lead to a loss of privacy and could possibly increase health-related disparities by allowing providers to characterize patients in more fine-grained ways. In the absence of effective legislation and regulation, patients may lack control over use of their data, leading to questions of whether autonomy, a key pillar of medical ethics, are being upheld. Overall though, we hope that our work leads to a net positive as it helps further the field towards creating personalized health recommendations, allowing patients to receive improved care and achieve better health outcomes, directly contributing to patient safety and overall well-being.

8 REPRODUCIBILITY STATEMENT

Our Methods section in Section 3 details the way in which we set-up our method, and our Experiments section in Section 4 details our experimental design. Additionally, in the Appendix A.3, we itemize each of the hyperparameters we used to tune each of our benchmarks. In the interest of anonymity, we have not yet released our Github code. Upon acceptance, we will release it to the public, which will have the set seeds and exact code we used to run our experiments. We will also make our model checkpoints downloadable. The datasets used are publicly available, and we describe how we curate each of them for our task in Appendix A.2, and upon acceptance, we will also release our specific data preprocessing code and direct data download.

REFERENCES

Sara Alaee, Ryan Mercer, Kaveh Kamgar, and Eamonn Keogh. Time series motifs discovery under dtw allows more robust discovery of conserved structure. *Data Mining and Knowledge Discovery*, 35:863–910, 2021.

Mathilde Caron, Hugo Touvron, Ishan Misra, Hervé Jégou, Julien Mairal, Piotr Bojanowski, and Armand Joulin. Emerging properties in self-supervised vision transformers. In *Proceedings of the IEEE/CVF international conference on computer vision*, pp. 9650–9660, 2021.

Ling Chen, Donghui Chen, Fan Yang, and Jianling Sun. A deep multi-task representation learning method for time series classification and retrieval. *Information Sciences*, 555:17–32, 2021.

Ting Chen, Simon Kornblith, Mohammad Norouzi, and Geoffrey Hinton. A simple framework for contrastive learning of visual representations. In *International conference on machine learning*, pp. 1597–1607. PMLR, 2020.

Xinlei Chen and Kaiming He. Exploring simple siamese representation learning. In *Proceedings of the IEEE/CVF conference on computer vision and pattern recognition*, pp. 15750–15758, 2021.

Mingyue Cheng, Qi Liu, Zhiding Liu, Hao Zhang, Ruijiao Zhang, and Enhong Chen. Timemae: Self-supervised representations of time series with decoupled masked autoencoders. *arXiv preprint arXiv:2303.00320*, 2023.

Jacob Devlin, Ming-Wei Chang, Kenton Lee, and Kristina Toutanova. Bert: Pre-training of deep bidirectional transformers for language understanding. *arXiv preprint arXiv:1810.04805*, 2018.

Emadeldeen Eldele, Mohamed Ragab, Zhenghua Chen, Min Wu, Chee-Keong Kwoh, Xiaoli Li, and Cuntai Guan. Self-supervised contrastive representation learning for semi-supervised time-series classification. *IEEE Transactions on Pattern Analysis and Machine Intelligence*, 2023.

Jean-Yves Franceschi, Aymeric Dieuleveut, and Martin Jaggi. Unsupervised scalable representation learning for multivariate time series. *Advances in neural information processing systems*, 32, 2019.

Jordan Frank, Shie Mannor, Joelle Pineau, and Doina Precup. Time series analysis using geometric template matching. *IEEE transactions on pattern analysis and machine intelligence*, 35(3):740–754, 2012.

Yash Garg and K Selçuk Candan. Sdma: Saliency-driven mutual cross attention for multi-variate time series. In *2020 25th International Conference on Pattern Recognition (ICPR)*, pp. 7242–7249. IEEE, 2021.

Shaghayegh Gharghabi, Shima Imani, Anthony Bagnall, Amiral Darvishzadeh, and Eamonn Keogh. Matrix profile xii: Mpdist: a novel time series distance measure to allow data mining in more challenging scenarios. In *2018 IEEE International Conference on Data Mining (ICDM)*, pp. 965–970. IEEE, 2018.

Priya Goyal, Dhruv Mahajan, Abhinav Gupta, and Ishan Misra. Scaling and benchmarking self-supervised visual representation learning. In *Proceedings of the IEEE/CVF International Conference on Computer Vision (ICCV)*, October 2019.

Yanchao Hao, Yuanzhe Zhang, Kang Liu, Shizhu He, Zhanyi Liu, Hua Wu, and Jun Zhao. An end-to-end model for question answering over knowledge base with cross-attention combining global knowledge. In *Proceedings of the 55th Annual Meeting of the Association for Computational Linguistics (Volume 1: Long Papers)*, pp. 221–231, Vancouver, Canada, July 2017. Association for Computational Linguistics. doi: 10.18653/v1/P17-1021. URL <https://aclanthology.org/P17-1021>.

Kaiming He, Haoqi Fan, Yuxin Wu, Saining Xie, and Ross Girshick. Momentum contrast for unsupervised visual representation learning. In *Proceedings of the IEEE/CVF conference on computer vision and pattern recognition*, pp. 9729–9738, 2020.

Kaiming He, Xinlei Chen, Saining Xie, Yanghao Li, Piotr Dollár, and Ross Girshick. Masked autoencoders are scalable vision learners. In *Proceedings of the IEEE/CVF conference on computer vision and pattern recognition*, pp. 16000–16009, 2022.

Seongsil Heo, Sunyoung Kwon, and Jaekoo Lee. Stress detection with single ppg sensor by orchestrating multiple denoising and peak-detecting methods. *IEEE Access*, 9:47777–47785, 2021.

Shichao Kan, Yigang Cen, Yang Li, Vladimir Mladenovic, and Zhihai He. Relative order analysis and optimization for unsupervised deep metric learning. In *Proceedings of the IEEE/CVF conference on computer vision and pattern recognition*, pp. 13999–14008, 2021.

Sungyeon Kim, Minkyo Seo, Ivan Laptev, Minsu Cho, and Suha Kwak. Deep metric learning beyond binary supervision. In *Proceedings of the IEEE/CVF Conference on Computer Vision and Pattern Recognition*, pp. 2288–2297, 2019.

Taesung Kim, Jinhee Kim, Yunwon Tae, Cheonbok Park, Jang-Ho Choi, and Jaegul Choo. Reversible instance normalization for accurate time-series forecasting against distribution shift. In *International Conference on Learning Representations*, 2021.

Dani Kiyasseh, Tingting Zhu, and David A Clifton. Clocs: Contrastive learning of cardiac signals across space, time, and patients. In *International Conference on Machine Learning*, pp. 5606–5615. PMLR, 2021.

Harim Lee, Eunseon Seong, and Dong-Kyu Chae. Self-supervised learning with attention-based latent signal augmentation for sleep staging with limited labeled data. In *Proceedings of the Thirty-First International Joint Conference on Artificial Intelligence, IJCAI-22, LD Raedt, Ed. International Joint Conferences on Artificial Intelligence Organization*, volume 7, pp. 3868–3876, 2022.

Kuang-Huei Lee, Xi Chen, Gang Hua, Houdong Hu, and Xiaodong He. Stacked cross attention for image-text matching. In *Proceedings of the European conference on computer vision (ECCV)*, pp. 201–216, 2018.

Hailin Li. Time works well: Dynamic time warping based on time weighting for time series data mining. *Information Sciences*, 547:592–608, 2021.

Zhe Li, Zhongwen Rao, Lujia Pan, Pengyun Wang, and Zenglin Xu. Ti-mae: Self-supervised masked time series autoencoders. *arXiv preprint arXiv:2301.08871*, 2023.

Zhengguang Li, Hongfei Lin, Chen Shen, Wei Zheng, Zhihao Yang, and Jian Wang. Cross2self-attentive bidirectional recurrent neural network with bert for biomedical semantic text similarity. In 2020 IEEE International Conference on Bioinformatics and Biomedicine (BIBM), pp. 1051–1054. IEEE, 2020.

Guilin Liu, Fitsum A Reda, Kevin J Shih, Ting-Chun Wang, Andrew Tao, and Bryan Catanzaro. Image inpainting for irregular holes using partial convolutions. In Proceedings of the European conference on computer vision (ECCV), pp. 85–100, 2018.

Yiwei Ma, Guohai Xu, Xiaoshuai Sun, Ming Yan, Ji Zhang, and Rongrong Ji. X-clip: End-to-end multi-grained contrastive learning for video-text retrieval. In Proceedings of the 30th ACM International Conference on Multimedia, pp. 638–647, 2022.

Antoine Miech, Jean-Baptiste Alayrac, Ivan Laptev, Josef Sivic, and Andrew Zisserman. Thinking fast and slow: Efficient text-to-visual retrieval with transformers. In Proceedings of the IEEE/CVF Conference on Computer Vision and Pattern Recognition, pp. 9826–9836, 2021.

George Moody. A new method for detecting atrial fibrillation using rr intervals. Proc. Comput. Cardiol., 10:227–230, 1983.

Isabelle Nault, Nicolas Lellouche, Seiichiro Matsuo, Sébastien Knecht, Matthew Wright, Kang-Teng Lim, Frederic Sacher, Pyotr Platonov, Antoine Deplagne, Pierre Bordachar, et al. Clinical value of fibrillatory wave amplitude on surface ecg in patients with persistent atrial fibrillation. Journal of interventional cardiac electrophysiology, 26:11–19, 2009.

Vit Niennattrakul, Dararat Srisai, and Chotirat Ann Ratanamahatana. Shape-based template matching for time series data. Knowledge-Based Systems, 26:1–8, 2012.

Manabu Okawa. Template matching using time-series averaging and dtw with dependent warping for online signature verification. IEEE Access, 7:81010–81019, 2019.

Aaron van den Oord, Yazhe Li, and Oriol Vinyals. Representation learning with contrastive predictive coding. arXiv preprint arXiv:1807.03748, 2018.

Yilmazcan Ozyurt, Stefan Feuerriegel, and Ce Zhang. Contrastive learning for unsupervised domain adaptation of time series. arXiv preprint arXiv:2206.06243, 2022.

James M Rehg, Susan A Murphy, and Santosh Kumar. Mobile Health: Sensors, Analytic Methods, and Applications. Springer, 2017. doi: 10.1007/978-3-319-51394-2.

Jorge Reyes-Ortiz, Davide Anguita, Luca Oneto, and Xavier Parra. Smartphone-Based Recognition of Human Activities and Postural Transitions. UCI Machine Learning Repository, 2015. DOI: <https://doi.org/10.24432/C54G7M>.

Patrick Schäfer and Ulf Leser. Motiflets: Simple and accurate detection of motifs in time series. Proceedings of the VLDB Endowment, 16(4):725–737, 2022.

Philip Schmidt, Attila Reiss, Robert Duerichen, Claus Marberger, and Kristof Van Laerhoven. Introducing wesad, a multimodal dataset for wearable stress and affect detection. In Proceedings of the 20th ACM international conference on multimodal interaction, pp. 400–408, 2018.

Sana Tonekaboni, Danny Eytan, and Anna Goldenberg. Unsupervised representation learning for time series with temporal neighborhood coding. International Conference on Learning Representations, 2021.

Ashish Vaswani, Noam Shazeer, Niki Parmar, Jakob Uszkoreit, Llion Jones, Aidan N Gomez, Łukasz Kaiser, and Illia Polosukhin. Attention is all you need. Advances in neural information processing systems, 30, 2017.

Patrick Wagner, Nils Strodtthoff, Ralf-Dieter Bousseljot, Dieter Kreiseler, Fatima I Lunze, Wojciech Samek, and Tobias Schaeffter. Ptb-xl, a large publicly available electrocardiography dataset. Scientific data, 7(1):154, 2020.

Haoran Wang, Dongliang He, Wenhao Wu, Boyang Xia, Min Yang, Fu Li, Yunlong Yu, Zhong Ji, Errui Ding, and Jingdong Wang. Coder: Coupled diversity-sensitive momentum contrastive learning for image-text retrieval. In *European Conference on Computer Vision*, pp. 700–716. Springer, 2022.

Gerald Woo, Chenghao Liu, Doyen Sahoo, Akshat Kumar, and Steven Hoi. Cost: Contrastive learning of disentangled seasonal-trend representations for time series forecasting. *arXiv preprint arXiv:2202.01575*, 2022.

Maxwell Xu, Alexander Moreno, Supriya Nagesh, Varol Aydemir, David Wetter, Santosh Kumar, and James M Rehg. Pulseimpute: A novel benchmark task for pulsative physiological signal imputation. *Advances in Neural Information Processing Systems*, 35:26874–26888, 2022.

Ling Yang and Shenda Hong. Unsupervised time-series representation learning with iterative bilinear temporal-spectral fusion. In *International Conference on Machine Learning*, pp. 25038–25054. PMLR, 2022.

Sitan Yang, Carson Eisenach, and Dhruv Madeka. Mqrettn: Multi-horizon time series forecasting with retrieval augmentation. *arXiv preprint arXiv:2207.10517*, 2022a.

Xinyu Yang, Zhenguo Zhang, and Rongyi Cui. Timeclr: A self-supervised contrastive learning framework for univariate time series representation. *Knowledge-Based Systems*, 245:108606, 2022b.

Yinfei Yang, Ning Jin, Kuo Lin, Mandy Guo, and Daniel Cer. Neural retrieval for question answering with cross-attention supervised data augmentation. *arXiv preprint arXiv:2009.13815*, 2020.

Chin-Chia Michael Yeh, Yan Zhu, Liudmila Ulanova, Nurjahan Begum, Yifei Ding, Hoang Anh Dau, Diego Furtado Silva, Abdullah Mueen, and Eamonn Keogh. Matrix profile i: all pairs similarity joins for time series: a unifying view that includes motifs, discords and shapelets. In *2016 IEEE 16th international conference on data mining (ICDM)*, pp. 1317–1322. Ieee, 2016.

Chin-Chia Michael Yeh, Yan Zhu, Liudmila Ulanova, Nurjahan Begum, Yifei Ding, Hoang Anh Dau, Zachary Zimmerman, Diego Furtado Silva, Abdullah Mueen, and Eamonn Keogh. Time series joins, motifs, discords and shapelets: a unifying view that exploits the matrix profile. *Data Mining and Knowledge Discovery*, 32:83–123, 2018.

Zhihan Yue, Yujing Wang, Juanyong Duan, Tianmeng Yang, Congrui Huang, Yunhai Tong, and Bixiong Xu. Ts2vec: Towards universal representation of time series. In *Proceedings of the AAAI Conference on Artificial Intelligence*, volume 36, pp. 8980–8987, 2022.

Hongjun Zhang, Jing Wang, Qinfeng Xiao, Jiaoxue Deng, and Youfang Lin. Sleeppriorcl: Contrastive representation learning with prior knowledge-based positive mining and adaptive temperature for sleep staging. *arXiv preprint arXiv:2110.09966*, 2021.

Xiang Zhang, Ziyuan Zhao, Theodoros Tsiligkaridis, and Marinka Zitnik. Self-supervised contrastive pre-training for time series via time-frequency consistency. *Advances in Neural Information Processing Systems*, 35:3988–4003, 2022.

Fuzhong Zheng, Weipeng Li, Xu Wang, Luyao Wang, Xiong Zhang, and Haisu Zhang. A cross-attention mechanism based on regional-level semantic features of images for cross-modal text-image retrieval in remote sensing. *Applied Sciences*, 12(23):12221, 2022.

A APPENDIX

A.1 REBAR APPROACH DETAILS

A.1.1 REBAR CROSS-ATTENTION DETAILS

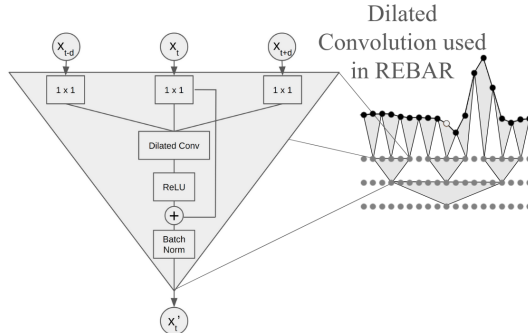


Figure 8: Dilated Convolution Block used in REBAR.

- **Dilated Convolution:** We use a modified version of the BDC transformer proposed in PulseImpute (Xu et al., 2022), which is visualized in Fig. 8. The batch norm has been replaced with an instance norm so that the model is not dependent on batch size to normalize the inputs. The bottleneck 1x1 layer reduces dimensionality, allowing for the model to be able to stack convolution layers with exponentially increasing dilation factors, thereby exponentially and efficiently increasing the receptive field. The residual connections are designed to help to facilitate more efficient training.
- **Positional embedding:** We opt to not use any positional encoding because we would like the retrieval function, $p(\mathbf{x}_k | \mathbf{\bar{x}}_q)$, to retrieve regions in the key subsequence based on similarity of the temporal shapes within the key and query in order to assess motif-similarity, rather than considering the specific positions of such structures. Additionally, knowing the exact positions is uninformative due to the arbitrary time at which sensors begin recording or are segmented. Thus, we seek to instead model relative position through the convolutions that can capture a subsequence’s shape.
- To handle masking, we utilize partial convolutions that ignore the calculation at masked points (Liu et al., 2018).
- An instance norm is used to normalize the query and key inputs with respect to the query, then is reversed at the end for reconstruction (Kim et al., 2021).

A.1.2 MASKING VALIDATION

Our REBAR cross-attention model compares the motifs within a specific receptive field around a masked time-point in the query sequence with the motifs in the key sequence. Then, it retrieves the best matching motif from the key to be used for reconstruction of that specific masked time-point in the query, and this idea is illustrated in the new Fig. 1 and Fig. 3.

At training time, a contiguous mask is used so that the model learns to compare specific, potentially class-discriminative, motifs in the query with specific, potentially class-discriminative, motifs in the key, rather than comparing minor, transient, non-unique motifs. See Fig. 4a) and b) for attention weight visualizations.

At application time, a contiguous mask could be used, however, in doing so, only the motifs near the contiguously masked out region would be compared to the key. This is because when reconstructing a given masked time-point and another point contiguous to it, the receptive fields to be used to identify motifs to be compared to the key are heavily overlapping. An intermittent mask allows for many different motifs in the query, each of them captured in a receptive field around the many masked time-points dispersed throughout the signal, to be compared to the key during reconstruction. This

allows for a higher coverage of the query in conducting such motif-similarity comparisons with the key. Therefore, during application, when we are testing each candidate as the key for a given anchor as the query, we would be able to identify the candidate which is most similar to the anchor as a whole.

Training Mask Type	Contiguous	Contiguous	Intermittent	Intermittent
Evaluation Mask Type	Contiguous	Intermittent	Intermittent	Contiguous
Accuracy	0.3624	0.4580	0.2888	0.2378

Table 4: Comparison of Different Masking Procedures for REBAR. The accuracy reported is from the validation strategy explicated in Section 3.4, applied to the PPG dataset, averaged across all classes.

As we see above, Training Contiguous + Application Intermittent achieves the best performance in our validation experiment, followed by Training Contiguous + Application Contiguous, then Training Intermittent + Application Intermittent, then Training w/ Intermittent + Application Contiguous. An intermittent mask preserves more information about the surrounding context of a masked out query point compared to a contiguous mask, and we see that a model trained with a contiguous mask can still reconstruct a signal masked with an intermittent mask in Fig. 4b) (the vice versa would not likely be true and is reflected in the empirical results).

A.1.3 HYPERPARAMETER ANALYSIS

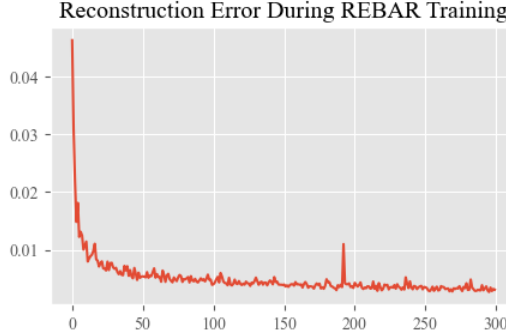


Figure 9: As the REBAR Cross-attention trains with the contiguous mask, reconstruction error decreases

	Acc	AUROC	AUPRC	ARI	NMI
Baseline at Epoch 300, Mask=15, RF=43					
REBAR	0.9535	0.9965	0.9891	0.6258	0.7721
Failure Cases (Lower is better)					
REBAR at Epoch 1	0.9437 (-0.010)	0.9954 (-0.001)	0.9841 (-0.005)	0.3635 (-0.290)	0.5213 (-0.251)

Table 5: REBAR model Failure Cases on HAR data

Effect of Proportion of Masking: The model is fairly robust against the size of the contiguous masks to be used for training the REBAR model. In our ablation study in Tbl. 3, compared to an initial mask size of 15, we found that using a smaller mask size of 5 time-points lowered accuracy by only 0.004 and using a larger mask size of 25 increased accuracy by .006.

For each of the datasets, the size of the contiguous mask is chosen to be large enough to mask out a potentially class-discriminative motif. This is done so that the model learns how to specifically retrieve this class-discriminative motif from the key and so that during evaluation, class-discriminative motifs between the key and query are compared. However, the mask size cannot be too large, because then even if the query and key are of the same class, it would be more difficult to precisely match a much larger motif with the increased noisiness

Thus, contiguous mask size can be tuned with a hyperparameter grid search or with expert domain knowledge. In HAR, it is a mask that covers .3 seconds (15 time-points) because the accelerometry

type data typically captures information of movement from short quick jerks. In PPG, it is a mask that covers 4.69 seconds (300 time points), which we do because PPG wave morphology is relatively simple, so we would like to capture a few quasi-periods. In ECG it is a mask that covers 1.2 seconds (300 time points), which covers a heartbeat, and ECG wave morphology is generally very descriptive and specific (e.g. QRS complex).

Effect of Dilated Convolution Receptive Field Size: This also helps guide the size of the receptive field that our dilated convolutions in our cross-attention should be. In general, we aim for the size of the receptive field to be three times the size of the contiguous mask, so that during training, the query dilated convolution would be able to effectively capture the motif surrounding the masked out query region to learn our cross-attention model. Additionally, as we see in the Tbl. 3, our model is robust to the exact receptive field size. Compared to an initial receptive field of 43, a receptive field of 31 decreases accuracy by only .003 while increasing ARI by .013 and a receptive field of 55 decreases accuracy by only .016 while increasing ARI by .031.

Effect of Reconstruction on Downstream Performance: Tbl. 3 shows that REBAR is robust to the hyperparameter of Number of REBAR Cross-Attn Epochs Trained. Fig. 9 in the Appendix shows that reconstruction error decreases as epochs trained increases, so reconstruction accuracy is not necessarily an indicator of downstream performance. This is not an issue because the REBAR Cross-attn’s goal within a contrastive learning framework is not to achieve a good reconstruction. Instead, we would like the REBAR Cross-attn to learn a good retrieval and motif-comparison function between the query and the key that achieves better or worse reconstruction, based on motif similarity. As noted in Section 3.1, we intentionally keep the design of REBAR attention simple to emphasize the motif comparison within the cross-attention mechanism. We note that these results should not imply that the REBAR model should not be trained. Tbl. 5 in the Appendix shows that if REBAR is only trained for 1 epoch, then accuracy drops by 0.010 and NMI drops by 0.251.

A.2 DATASET DETAILS

The time-series are split into a 70/15/15 train/val/test split. We note that below the total time coverage of the class-labeled subsequences does not equal to the total time coverage of the time-series that they are segmented from, because some of the datasets contain parts that were unlabeled.

HAR: Rather than using the extracted time and frequency features, we opt to use the raw accelerometer and gyroscopic sensor data (Reyes-Ortiz et al., 2015) to better assess how our methods perform on raw time-series. Our subsequences are 2.56-second-long (128 time points) to match the subsequence length proposed for classification in the original work (Reyes-Ortiz et al., 2015). There are 6,914 distinct subsequences total for training and testing our models, which are sampled from 59 5-minute-long (15,000) time-series that are sampled at 50 Hz and has 6 channels. There are 4,600 class-labeled subsequences, with the following labels: walking (17.7%), walking upstairs (7.6%), walking downstairs (9.1%), sitting (18.2%), standing (20.1%), and laying (20.1%).



Figure 10: Example of one channel of HAR Signal

PPG: From the WESAD dataset (Schmidt et al., 2018), we use 1-minute-long (3840 time points) subsequences to match the subsequence length proposed in the original work (Schmidt et al., 2018). There are 1,305 distinct subsequences total for training and testing our models, which are sampled from 15 87-minute-long (334,080 time points) time-series, sampled at 64 Hz with a single channel. There are a total of 666 class-labeled subsequences, with the following labels: the labels are baseline (42.7%), stress (24.0%), amusement (12.4%), and meditation (20.9%). The data has been denoised following the procedure in Heo et al. (2021).

ECG: From the MIT-BIH Atrial Fibrillation dataset (Moody, 1983), we use 10-second-long (2500 time points) subsequences. The original work (Moody, 1983) does not have a proposed subsequence

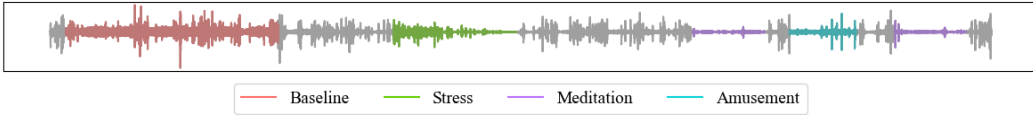


Figure 11: Example of PPG Signal

length, so we use this 10-second-long subsequence length to match the prior work for this dataset (Tonekaboni et al., 2021) and the 10-second-long length used in general ECG classification works (Wagner et al., 2020). There are 76,590 distinct subsequences total for training and testing our models, which are sampled from 23 9.25-hour-long (8,325,000 time points) time-series sampled at 250 Hz with dual channels. There is a total of 76,567 10-second-long (2500 time points) class-labeled subsequences, with the following labels: atrial fibrillation (41.7%) and normal (58.3%). These subsequences originate from 23 9.25-hour-long (8,325,000 time points) time-series sampled at 250 Hz with dual channels.

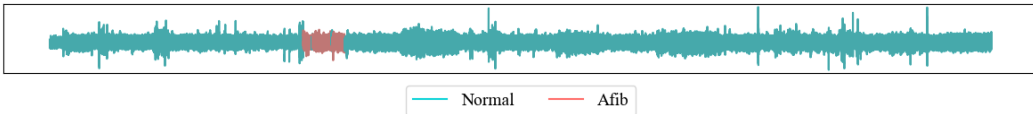


Figure 12: Example of one channel of ECG Signal

A.2.1 DISCUSSION ABOUT UCR/UEA TIME-SERIES DATABASE

We note that we opt to not benchmark on the commonly utilized UCR and UEA time-series dataset databases, as they do not because they do not fit our stated problem area of time-series that are series of class-labeled subsequences, would prevent us from benchmarking sampling-based contrastive learning methods, and many of datasets found within the databases are very small.

Our work is framed for long time-series data that can be described as a series of class-labeled subsequences, rather than a collection of short class-labeled time-series (e.g. UCR, UEA). For context, our datasets have time-series that are 8,325,000 / 334,080 / 15,000 time points long, compared to the median length of 621 and 301 for UEA and UCR respectively. Our defined subset of time-series data is the closest primitive to true time-series sensors, in which sensors are designed to collect large volumes of unlabeled data continuously and autonomously. We note that this setting particularly describes the physiological sensor time-series domain, in which the advancement of wearable technologies has enabled large data collection on a user’s changing physiological states, but the cost of labeling remains high (i.e. mHealth sensors require constant user annotation and clinical sensors require medical expertise). Hence, we believe that this particular time-series domain has the largest opportunity for impact in the ML and greater health community.

Using this type of long time-series data in our problem also allows us to benchmark sampling-based contrastive learning methods, such as TNC (Tonekaboni et al., 2021) and our own REBAR method. These sampling-based methods fully exploit the time-series nature of our task. Because each subsequence is part of a specific user’s sensor time-series that is changing over time, we can sample positive and negative examples directly from the larger time-series, rather than attempting to create positive examples from augmentations. Unfortunately, the datasets that support this type of task are limited: TNC only included HAR, ECG, and a small simulated dataset. Our work adds the PPG dataset for stress classification, to introduce a new benchmark dataset for this type of time-series contrastive learning task.

Additionally, many of the datasets within UEA and UCR may not suitable for evaluating self-supervised learning, due to their small sizes. Self-supervised learning has risen into prominence due to how it exploits large-scale unlabeled datasets, and such methods have been found to be sensitive to dataset size (Goyal et al., 2019). However, 90 out of the 128 datasets in UCR and 123 out of the 183 datasets in UEA have 1,000 or less sequences to train a model. 8 out of the 128 total

datasets in UCR and 14 out of the total 183 total datasets in UEA have less 100 or less sequences. After segmenting our time-series into the contiguous subsequences that are used to train each of our self-supervised learning models, we have a total number of 76,590 / 6,914 / 1,305 sequences for ECG, HAR, and PPG, respectively.

A.3 BENCHMARK IMPLEMENTATIONS

All of our code with the model implementations and evaluations, along with trained checkpoints and the set seed, will be made publicly available for reproducibility. We use the validation set to choose the best model checkpoint to be evaluated on the test set, and tune each model’s hyperparameters to achieve its best performance.

For the non-sampling-based methods (i.e. TS2Vec, CPC, SimCLR), we train these methods on subsequences. The subsequences sizes used during the contrastive learning stage match the downstream subsequence sizes used for classification: length 128 for HAR, length 3840 for PPG, and length 2500 for ECG. The encoder is kept constant across each of our methods, and we used the dilated convolution encoder from TS2vec (Yue et al., 2022) with an embedding size of 320.

- Fully Supervised uses the same encoder and linear classification head, trained with a class balanced weights and cross entropy loss, identical to all of the other linear probe models, only trained end-to-end
 - Each of the domains were trained with a learning rate of .00001 until convergence
- TS2Vec (Yue et al., 2022) is a current state-of-the-art time-series contrastive learning method that learns time-stamp level representations with augmentations.
 - We follow the default implementation used in <https://github.com/yuezhihan/ts2vec>. In PPG, we have a learning rate of .0001 and batch size of 16, in ECG, we have a learning rate of 0.00001 and batch size of 64, and in HAR, we have a learning rate of 0.00001 and batch size of 64.
 - Our reported TNC results for HAR are higher than the original reported results because, we use TS2Vec’s proposed dilated convolution encoder, and in order to fairly compare all of the contrastive learning baselines, we keep this encoder backbone constant across all of the baselines. In TNC’s original work, they used a simpler RNN model for the HAR data. TSVec also found that training TNC with the dilated convolution encoder achieves better results (See Appendix C.3 in (Yue et al., 2022)). Additionally, other discrepancies may originate from how TNC evaluated their method by training a classification head with the encoder model end-to-end, rather than freezing the encoding. We opt to freeze the encoder in order to allow for the encoded representation to be directly evaluated via a linear classifier (i.e. Acc, AUROC, AUPRC) and clusterability (i.e. Adjusted Rand Index and Normalized Mutual Information). We have added these details into the Appendix A.3
- TNC (Tonekaboni et al., 2021) samples a nearby subsequence as a positive and utilizes a hyperparameter to estimate whether a faraway sampled subsequence is a negative.
 - We follow the default implementation used in https://github.com/sanatonek/TNC_representation_learning and set w to .2. in PPG, we have a learning rate of .0001 and batch size of 16, in ECG, we have a learning rate of .001 and batch size of 16, and in HAR, we have a learning rate of .00001 and a batch size of 16. At the end of the encoder, we utilize a global max pooling layer to pool over time.
- CPC (Oord et al., 2018) contrasts based on future timepoint predictions.
 - We follow the default implementation used in <https://github.com/jefflai108/Contrastive-Predictive-Coding-PyTorch>. For PPG, we have a learning rate of .001 and batch size of 16, for ECG, we have a learning rate of .001 and batch size of 16, and for HAR, we have a learning rate of .001 and a batch size of 64.
- SimCLR (Chen et al., 2020) is a simple augmentation-based method we have adapted for time-series. The most common time-series augmentations are used (i.e. shifting, scaling, jittering), allowing us to assess how suitable a pure augmentation-based strategy is.
 - We have 3 augmentations: scaling, shifting, and jittering, with each of the three having a 50% probability of being used. Scaling multiples the entire time-series with a number uniformly sampled from 0.5 to 1.5. Shifting will shift the time-series by a random number between -subsequence_size to subsequence_size. Jittering will add a random gaussian noise to the

signal, with the gaussian noise’s standard deviation set to .2 of the standard deviation of the values in the entire dataset. For PPG, we have a learning rate of .001, τ is 1, and batch size of 16, for ECG, we have a learning rate of .001, τ is 1, and batch size of 16, and for HAR, we have a learning rate of .001, τ is 1, and batch size of 64. At the end of the encoder, we utilize a global max pooling layer to pool over time.

- Sliding-MSE is a simpler version of REBAR, in which a simple method is used to assess the similarity of a pair of sequences. We slide the candidate subsequence, padded with the true sequence values, along the anchor subsequence and calculate MSE at each iteration. The lowest MSE of the slide is then used as our metric to label the positive and negative examples.
 - For PPG, we have a learning rate of .001, 20 sampled candidates, and τ is 1000, for ECG, we have a learning rate of .1, 20 sampled candidates, and τ is 1000, and for HAR, we have a learning rate of .001, 20 sampled candidates, and τ is 0.1. At the end of the encoder, we utilize a global max pooling layer to pool over time.
- REBAR is our REtrieval-BAsed Reconstruction method for time-series contrastive learning
 - Our cross-attention model was trained to convergence and the bottleneck dilated convolution block has an embedding size of 256 channels, initial kernel size of 15 and dilation of 1 and then the dilation gets doubled for each following layer. The input channel size of the first convolution is equivalent to the number of channels present in the data, and the bottleneck layer has an embedding size of 32. For the PPG and ECG datasets, we have 6 dilated convolution layers to capture a larger receptive field of 883 and for the HAR dataset, we have 2 layers to capture a receptive field of 43. During training, our contiguous mask sizes for PPG, ECG, and HAR are 300, 300, and 15 respectively. During evaluation, the intermittent mask masked out 50% of the time points of the signal. During contrastive learning, for PPG data, we have a learning rate of .0001, 20 sampled candidates, τ is 10, and batch size of 16, for ECG, we have a learning rate of .1, 20 sampled candidates, τ is 1, and a batch size of 16, and for HAR, we have a learning rate of .001, 20 sampled candidates, τ is 1, and a batch size of 64. At the end of the encoder, we utilize a global max pooling layer to pool over time.

A.4 CONNECTING POSITIVES TOGETHER AND FALSE NEGATIVES

False negatives are fundamental issue within contrastive learning more broadly and are not specific to our REBAR method. For example, in augmentation-based approaches like SimCLR (Chen et al., 2020), they sample negative items from the batch, and the batch may contain items from the same downstream classification category as the anchor. However, they are able to still achieve strong performance. Similarly, our approach is still able to achieve the best representation learning performance across our baselines. One idea to address this could be a thresholding method, but we believe that this method would be ineffective. A threshold should not be designed to be a hyperparameter as it would be dependent on how each specific anchor’s specific motifs compare to other general instances within the same class. However, learning a threshold as a function of the anchor is not obvious to do, due to the lack of class label ground truth during contrastive learning.

Addressing false negatives is an ongoing research area. Our current implementation utilizes the REBAR metric to binarize candidates into positives and negatives, but future work could explore how to directly use the REBAR metric such that the distance of pairs in embedding space reflects the difference of their REBAR metrics, similar to what was done in the Log-ratio Loss (Kim et al., 2019). Alternatively, the relative order of the candidates given by REBAR can be enforced, by using methods such as ROUL (Kan et al., 2021).

A.5 EXTRA VISUALIZATIONS FOR POSITIVE PAIRS

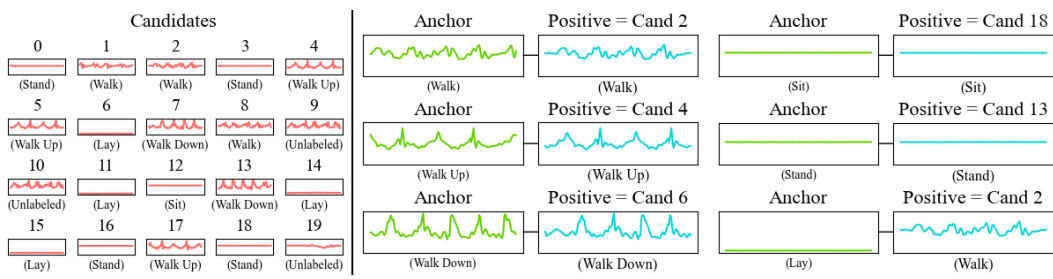


Figure 13

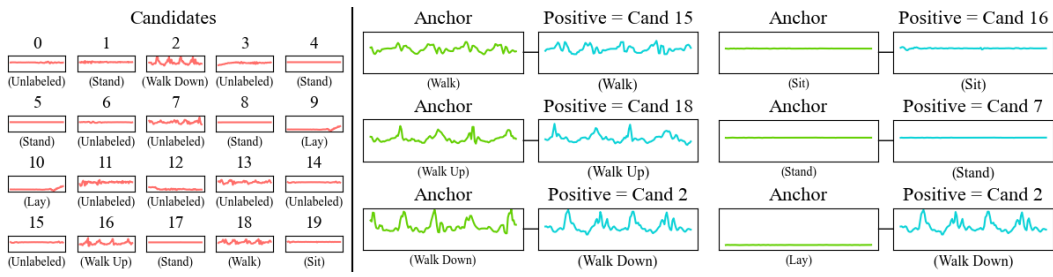


Figure 14

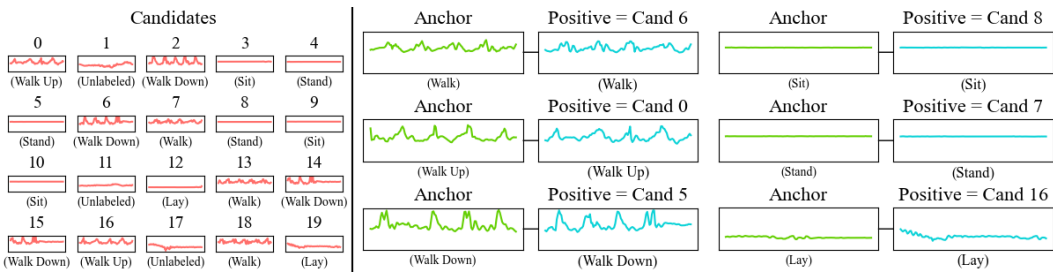


Figure 15

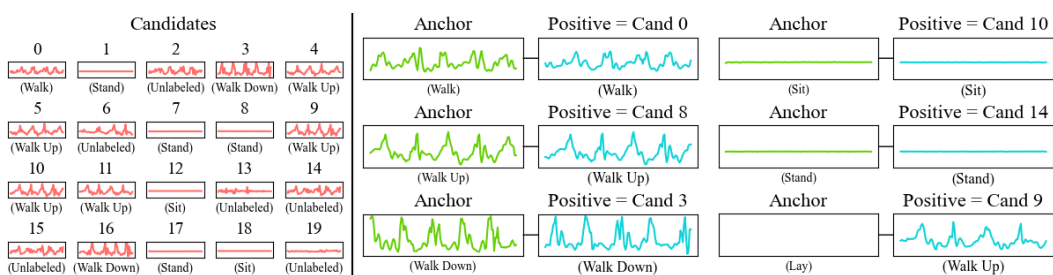


Figure 16

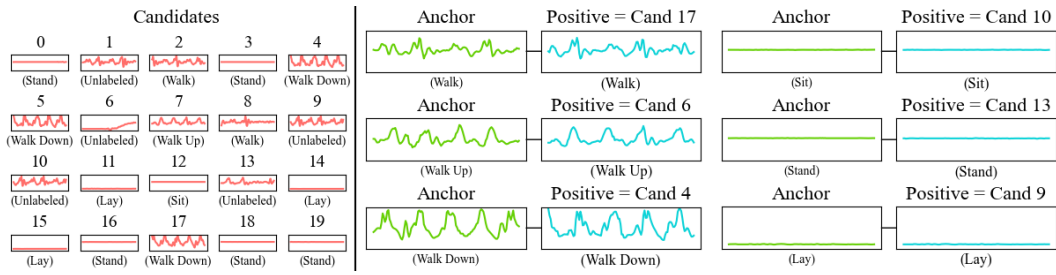


Figure 17

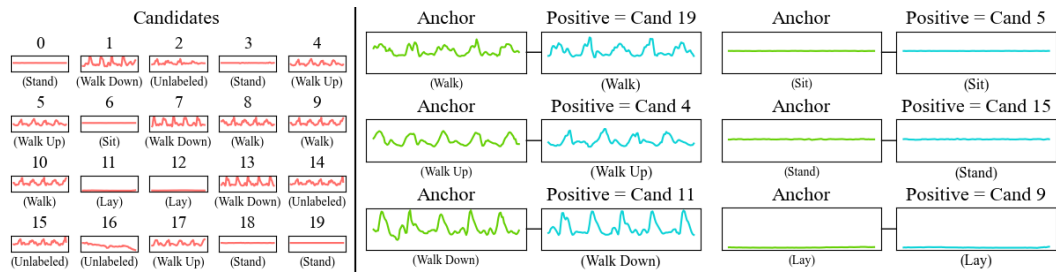


Figure 18

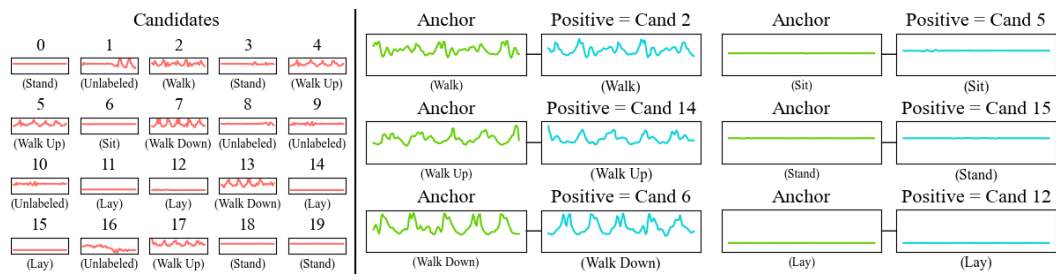


Figure 19

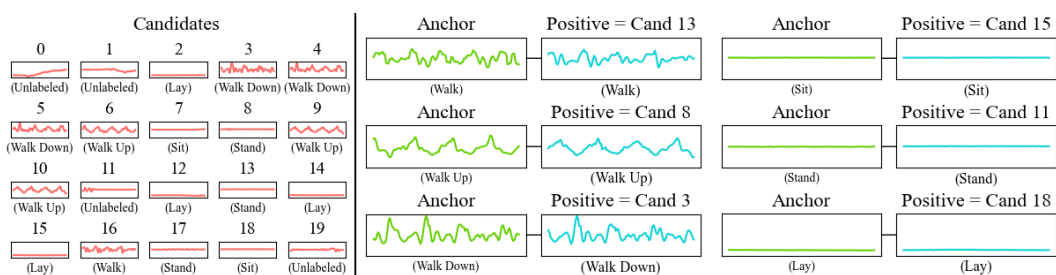


Figure 20

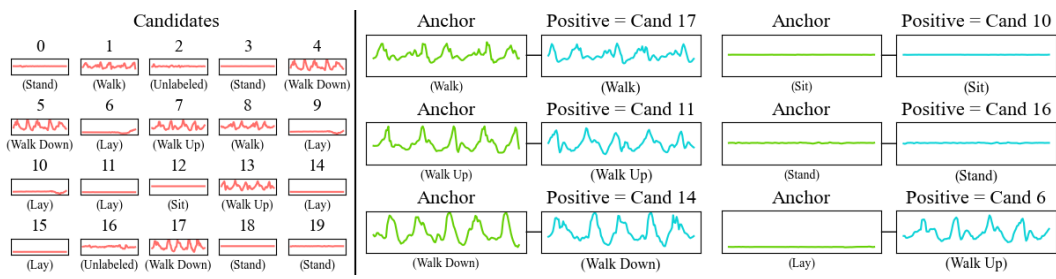


Figure 21

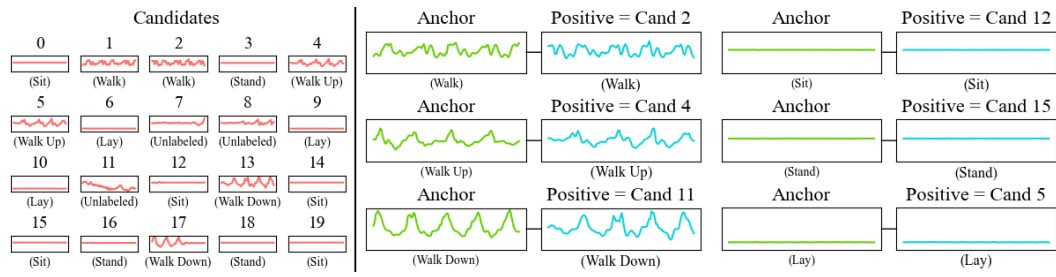


Figure 22

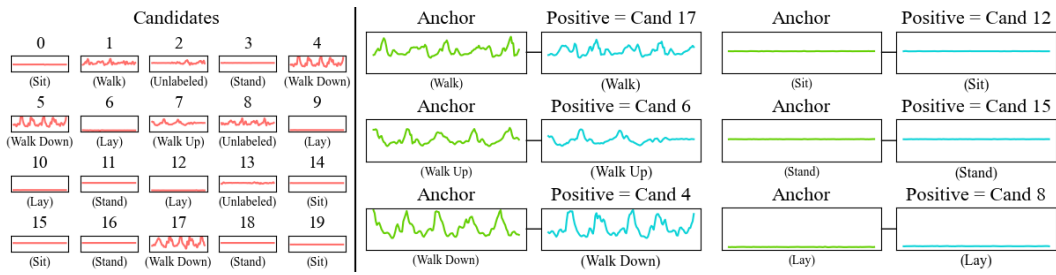


Figure 23

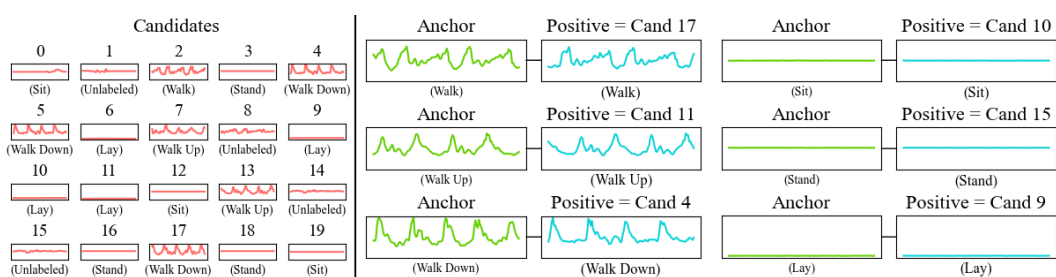


Figure 24

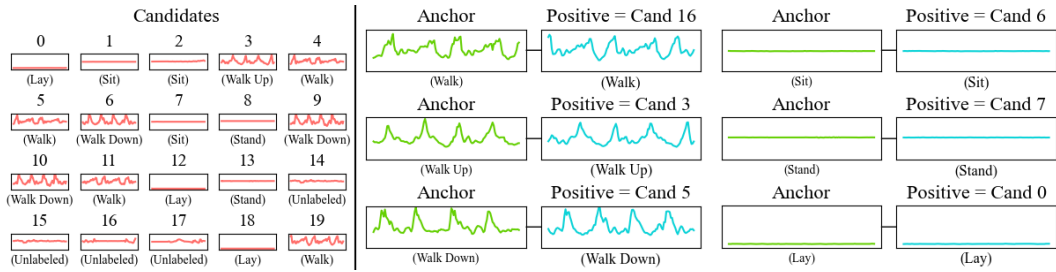


Figure 25

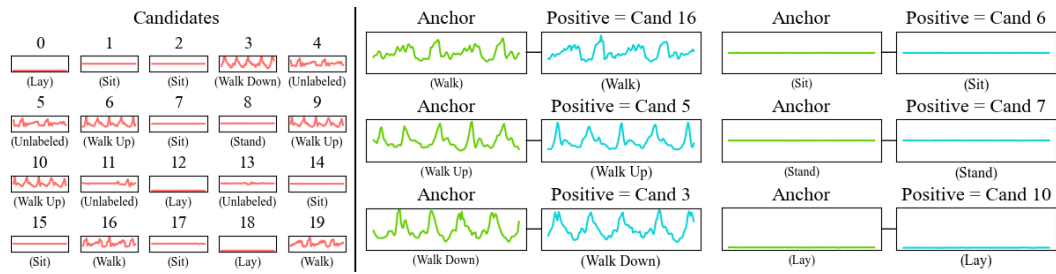


Figure 26

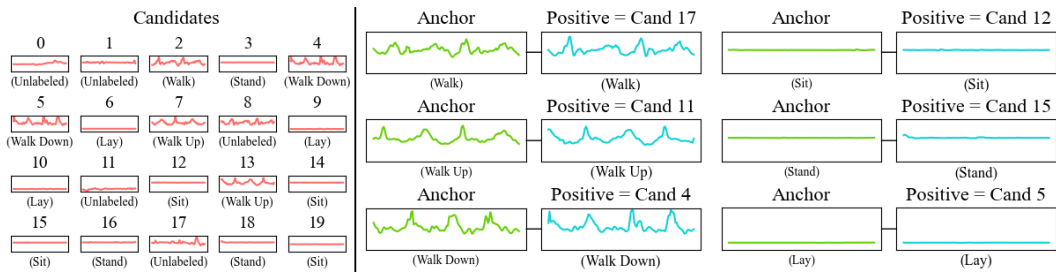


Figure 27